17th International Conference
ENGINEERING MECHANICS 2011
Svratka, Czech Republic, 9 – 12 May 2011

FAILURE MECHANISM AND STRAIN FIELDS ON A CARBON/EPOXY COMPOSITE SUBJECTED TO COMPRESSION AFTER IMPACT

M. Kadlec*

Abstract: *Polymer composite panels are widely used in aeronautic and aerospace structures due to their high strength vs. weight ratio. The objective of this study is to determine mechanisms of the failure of impacted composite laminates when subjected to compression. The other aim is to investigate using an optical strain measurement to detect impact damage in laminates subjected to loading. For this purpose a series of impact and compression after impact (CAI) tests were carried out on composites made of carbon fibre-reinforced epoxy resin matrix. First, impacted specimens were analyzed by an ultrasonic probe to assess delamination area around the impact site. Second, digital image correlation (DIC) measurement was performed to investigate the strain fields and the surface shape before and during loading. The full-field strain measurements showed a concentration band of a compressive strain near the impact where buckling occurred. The shear strain visualisation around the impact showed an area of heterogeneous deformation which was compared to the detected delamination area acquired by an ultrasonic technique. The results showed that the shear strain fields are able to identify the extension of impact damage and that the strain concentration factor can be a failure criterion to consider an ultimate load.*

Keywords: ***Polymer composite, compression, strain field, impact damage, digital image correlation.***

1. Introduction

Impact damage is serious damage mechanism in polymer composite laminates which limits its performance and reliability. It can occur during in-service or as a result of handling during manufacture. This can give rise to surface indentations and other damage below the surface such as matrix cracking, fibre breakage, delamination or disbonding. Under compressive loads, these failure mechanisms interact and compared to the undamaged state the impact-induced damage propagates to failure at significantly lower load levels (Cantwell, et al., 1986).

Paper (Freitas & Reis, 1998) described two buckling failure mechanisms (positive and negative impact site out-of-plane displacement) which are influenced more by the delamination area than by the stacking sequence. Sutherland et al. (2005) predicted the damage initiation threshold using two models, one based on the interlaminar fracture toughness of the composite and the second on the interlaminar shear strength ILSS. Yang, et al (2010) showed that the latter can successfully predict the relation of critical force to both target size and impactor geometry. The numerical results in the paper (Yan et al., 2010) denoted an extensive propagation of delamination with mode transition preceding sublaminate buckling. Initiation and propagation of matrix and fiber cracking, observed upon this buckling, is the cause of ultimate shear failure. The paper (Petit et al., 2007) presented CAI tests performed on composite laminate covered with a cork thermal shield. They investigated out-of-plane displacement field around the impacted zone by using two CCD cameras.

This paper deals with pure panels where are investigated not only the displacements, but also strains around the impacted zone by using photogrammetric system ARAMIS. The strain values before failure inside the impact zone are used for strain concentrations calculations. The second part of the results show visualizations of the shear strains in comparison with the ultrasound detected delamination areas.

* Ing. Martin Kadlec: Aeronautical Research and Test Institute (VZLÚ, a.s.), Beranových 130; 199 05 Prague; CZ, e-mail: kadlec@vzlu.cz

2. Methods

Composite laminate specimens with dimensions 150 x 100 x 4 mm were manufactured by dry tows placement of IMA GS carbon fibres with areal weight of 140 g/m^2 and fibre volume of 57 %. The SDV32 resin system was introduced by injection. The lay-up configuration was $[0/45/90/-45]_{4s}$.

All the 4 specimens were impacted by 16 mm diameter 5450 g mass impactor with energy 35 J. Fig. 1 shows an arrangement of an impact test including the clamp system which held the specimens. The impact machine prevented multiple hits on the specimen. Non-destructive detection of delaminations by Masterscan 340 ultrasound system with direct probe PRDT 2550, 5 Mhz was carried out after impacting and before loading. The delamination area was measured in 8 directions from the impact centre.

The antibuckling fixture (Fig. 2a) was used for loading according the AITM 1.0010 specification. The compressive loading was performed by SCHENCK 250 kN with constant displacement of 0.5 mm/min. ARAMIS HS system for full-field strain measurements is shown in Fig. 2b.

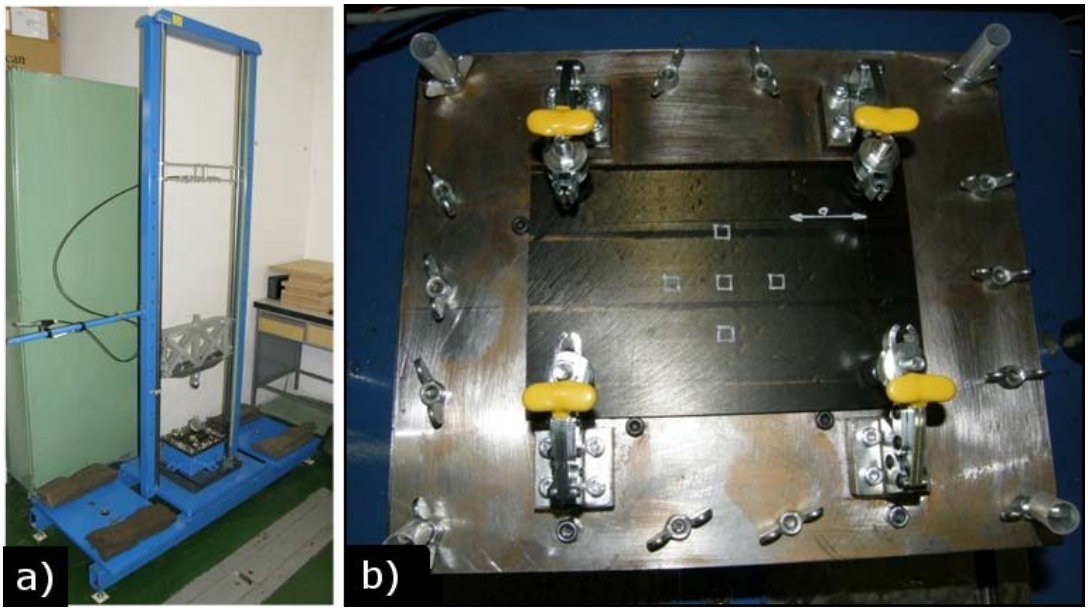

Fig. 1: a) Impact machine set up. b) Clamping device for impacting system with a specimen.

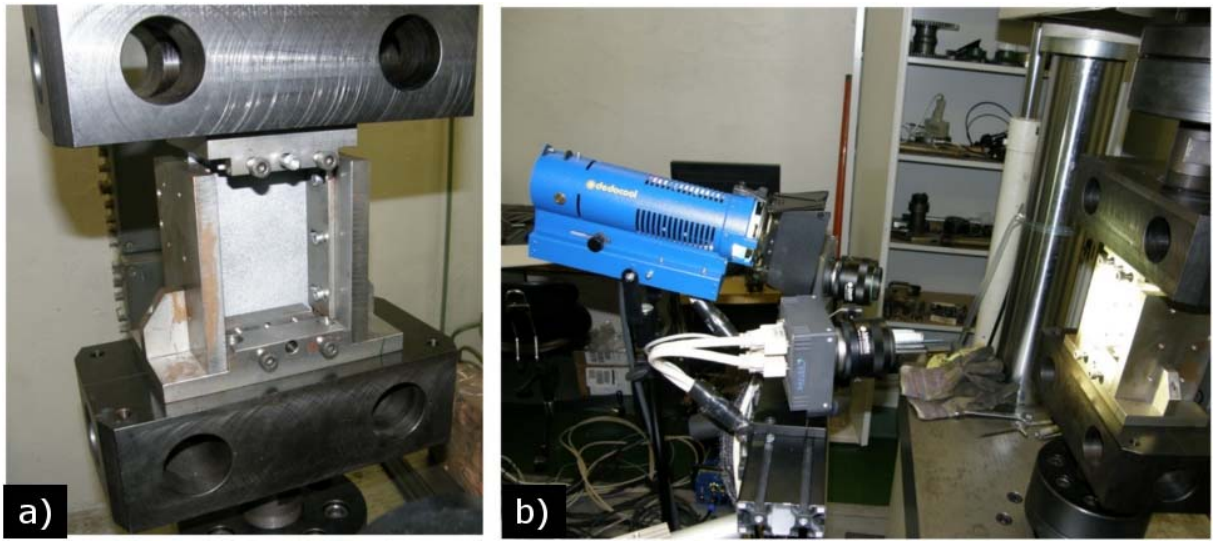

Fig. 2: a) CAI antibuckling fixture with a specimen sprayed by a black-white pattern.
b) The ARAMIS cameras and a light aiming at a specimen.

3. Results

Impact dent depth and shape were measured by DIC and processed in MATLAB (Fig. 3). The mean depth value for the tested specimens was 0.29 mm.

Failure by loading was sudden without crack propagation. The fracture was observed in the plane perpendicular to the loading and passing through the impact dent where the compressive strain concentrations were dominant. The measured strain fields on specimen "A" before failure are shown in the following figures. Fig. 4a shows a field of strain in the loading direction with contraction of the impact depression and elongation of its borders. Fig. 4b represents shear strain in the specimen plane. The typical cross visualisation reveals the dent position and the affected area by the impact. Fig. 5a shows a field of von Mises strain which reveals also the cracks from impacting. Fig. 5b demonstrates the out-of-plane displacement and shows the further recessing of the dent during loading.

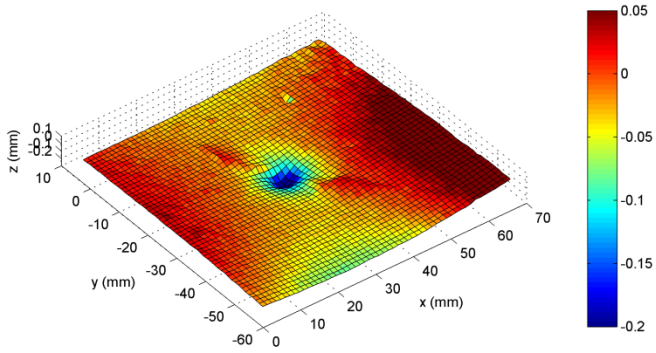

Fig. 3: The middle part of the specimen "A" surface after impact. Two diagonal cracks are visible. Z axis is 20 times scaled.

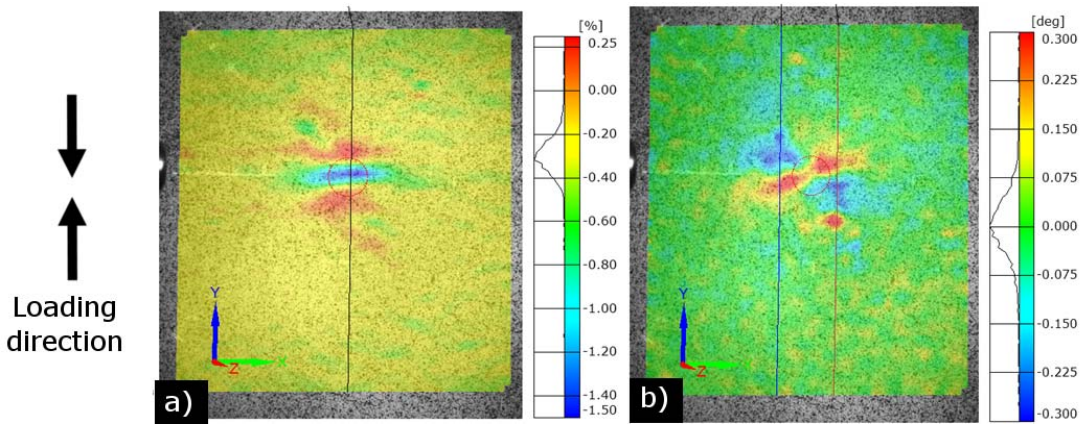

Fig. 4: a) Field of vertical strain ε_y before failure. b) Field of shear angle before failure.

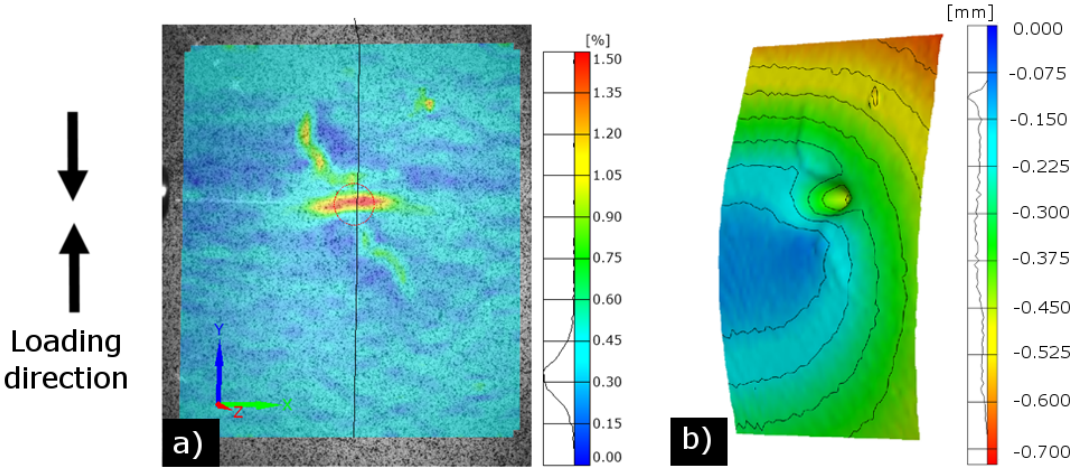

Fig. 5: a) Field of von Mises strain with visible cracks from impacting.
b) Buckling visualized as out-of-plane displacement field scaled 10 times.

Compression strength σ_d was obtained by division of maximum force F_{max} and specimen edge surface. Strain concentration factor was suggested as

$$\alpha_M = -\varepsilon_M/\varepsilon_A\,, \tag{1}$$

where ε_M is local von Mises strain at the impact centre and ε_A is averaged surface strain of the plate in the loading direction far from the impact. Both the strains were measured before failure. All the mentioned quantities are included in Tab. 1.

Tab. 1: Strength, strain before failure and calculated strain concentration factors.

Specimen	F_{max} (kN)	σ_d (MPa)	ε_A (%)	ε_M (%)	α_M (1)
A	76.96	191.22	-0.30	1.95	6.5
B	78.42	193.62	-0.29	1.83	6.3
C	98.69	241.60	-0.36	2.15	6.0
D	102.38	256.32	-0.36	2.40	6.7

The shear strain visualisation was thresholded by the value of 0.06˚ to reveal the damage induced heterogenity of the material. For comparison, the ultrasound detected delamination area border was overlaid to proof the fact, a delamination range can be detected by strain measurements (Fig. 6).

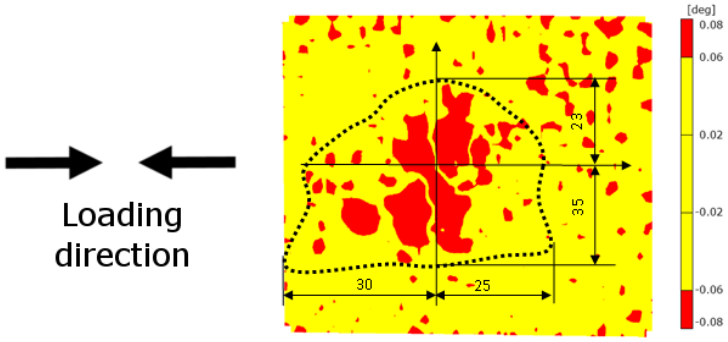

Fig. 6: Thresholded field of shear strain with the overlaid border of ultrasound detected delamination.

4. Conclusions

The strain concentration coefficients are in a very good agreement in spite of the fact that the strengths are different which suggests it can be the failure criteria for compression after impact loading. The shear strain visualisation corresponds to a delamination extent in this composite material.

Acknowledgement

Financial support of grant MSM 0001066903 from the Czech Ministry of Education, Youth and Sport is gratefully acknowledged. The author also acknowledges Mr. Valerij Makarov for NDT measurements.

References

Cantwell, W.J., Curtis, P. & Morton, J. (1986) An assessment of the impact performance of CFRP reinforced with high-strain carbon fibers. Compos Sci Technol, 25, pp.133–148.

Freitas, M. & Reis, L. (1998) Failure mechanism on composite specimens subjected to compression after impact. Composite Structures, 42, pp.365-373.

Petit, S., Bouvet, C., Bergerot, A. & Barrau, J. (2007) Impact and compression after impact experimental study of a composite laminate with a cork thermal shield. Compos Sci Technol, 6, pp.3286-3299.

Sutherland L.S. & Guedes S.C. (2005) Contact indentation of marine composites. Composite Structures, 70, pp.287–94.

Yan, H., Oskay, C., Krishnan, A. & Xu, L.R. (2010) Compression-after-impact response of woven fiber-reinforced composites. Compos Sci Technol, 70, pp.2128-2136.

Yang, F.J. & Cantwell, W.J. (2010) Impact damage initiation in composite materials. Compos Sci Technol, 70, pp.336-342.